University of Huddersfield Repository

Solano-Alvarez, Wilberth, Peet, M, Pickering, E, Jaiswal, Jay, Bevan, Adam and Bhadeshia, Harry

Synchrotron and neural network analysis of the influence of composition and heat treatment on the rolling contact fatigue of hypereutectoid pearlitic steels

Original Citation

This version is available at http://eprints.hud.ac.uk/id/eprint/33325/

http://eprints.hud.ac.uk/

Synchrotron and neural network analysis of the influence of composition and heat treatment on the rolling contact fatigue of hypereutectoid pearlitic steels

W. Solano-Alvarez[a,*], M.J. Peet[b], E.J. Pickering[c], J. Jaiswal[d], A. Bevan[d], H.K.D.H. Bhadeshia[a]

[a] Department of Materials Science and Metallurgy, University of Cambridge, UK
[b] Medical Research Council, Laboratory of Molecular Biology, Cambridge, UK
[c] School of Materials, University of Manchester, UK
[d] Institute of Railway Research, University of Huddersfield, UK

ARTICLE INFO

Keywords:
Synchrotron
Cementite dissolution
Hypereutectoid rail steels
Rolling contact fatigue
Neural network
Pearlite

ABSTRACT

A series of experimental hypereutectoid pearlitic steels were tested under rolling contact sliding conditions using a lubricated twin-disc setup to study the influence of different chemical compositions and heat treatments on rolling contact fatigue life. Tested samples were then characterised using microscopy and synchrotron measurements as a function of depth from the contact surface. Results, analysed through neural networks, indicate that the most influential factor in lengthening the number of cycles to crack initiation of hypereutectoid steels is hardness, attained by increasing the cooling rate from the hot rolling temperature, but adequate alloying additions can enhance it further. The harder, fast-cooled samples displayed less plastic flow at the surface than the softer slow-cooled ones. With regard to chemical composition, silicon was found to strengthen the ferrite thus reducing strain incompatibilities with the cementite, preventing in this way the fragmentation and eventual dissolution of the lamellae. This is beneficial since larger depths of cementite dissolution were found in samples with lower cycles to crack initiation for a given cooling rate (hardness). Samples containing vanadium lasted longer and displayed less plastic deformation at the surface than those without, at a similar hardness.

1. Introduction

Hypereutectoid rail steels (0.8–1.0 wt% C) are attractive for heavy haul applications as well as mixed traffic networks due to their higher resistance to wear and gross plastic deformation that derives mainly from their higher hardness in comparison to eutectoid C-Mn steel [1]. Despite many counterexamples [2–4], higher hardness in rail steels has been linked to a greater wear and rolling contact fatigue (RCF) resistance [5–8], which are the main degradation mechanisms of railway tracks during service. Nevertheless, head hardened rails of such a high carbon content can contain proeutectoid cementite, which has been shown to be detrimental to rolling contact fatigue life, fracture toughness, elongation, and wear resistance in rail steels [9–11]. The proeutectoid phase at the rail-wheel contact locations can be mitigated through controlled cooling ($>2.5\,°C\,s^{-1}$) from the finish rolling temperature [12] or a silicon addition in excess of about 0.8 wt% [9]. Silicon alloying has been recognised as a more reliable alternative to preventing grain boundary cementite since accelerated cooling rates may not be achieved by direct air impingement on rail heads, are depth

dependent, or may lead to martensite formation in the heavily segregated web region for cooling rates greater than $4\,°C\,s^{-1}$ [9]. In addition to carbon and silicon, high performance ultra-high carbon steels (UHC) can contain elements such as Mn, Cr, Ti, and V, whilst restricting others like N, P, and S, to achieve improved properties even in the relatively soft as-rolled condition (~ 370 HV), challenging the hardness based approach [9]. Such improvements have been attributed to interlamellar spacing refinement, increased cementite volume fraction, solid solution strengthening of ferrite [1,9], and precipitation strengthening through V/Ti carbides [13]. Since the improvements brought about through alloying are additive to the known benefits from higher cooling rates to increase hardness through refinement of interlamellar spacing, these steels can be heat treated to endure more demanding service conditions.

The aim of this work is to understand the specific role that each alloying addition or heat treatment (normal or accelerated cooling) has in determining certain microstructural parameters (hardness, interlamellar spacing, cementite volume fraction, ferrite lattice parameter) and identifying those most responsible for the overall wear and rolling contact fatigue performance of the alloy with the aid of numerical

Table 1
Chemical composition of twin-disc samples, wt%.

Grade	C	Mn	Si	Cr	V	Al	P	S	N	Ti	Others
AR + 0.3Cr	0.92	0.96	>0.40	0.32	0.004	0.002	0.008	–	–	–	Mo <0.005, Ni 0.031, Co 0.015, Cu 0.025, Sn 0.002, Pb <0.004
AR + 0.8Si + 0.1 V	0.92	0.88	0.79	0.06	0.14	0.005	0.012	0.007	0.011	0.013	
HT + 0.8Si + 0.1 V	0.92	0.88	0.79	0.06	0.14	0.005	0.012	0.007	0.011	0.013	
HT + 1.0Si + 0.1 V	0.94	0.84	0.96	0.05	0.13	0.006	0.011	0.005	0.009	0.013	
HT	0.99	1.09	0.56	0.21	–	<0.005	0.015	0.017	0.006	0.013	
Wheel	0.56	0.76	0.36	0.14	0.003	0.036	0.006	0.004	–	0.009	Mo 0.013, Ni 0.08, Cu 0.11, Nb 0.001, Sb 0.015, Sn 0.009

Table 2
Results from twin-disc testing and microstructural characterisation showing average values and standard error with a 95% confidence interval.

Rail sample	Cycles to initiation/10^3	Hardness rail / HV30	Hardness wheel / HV20	True interlamellar spacing rail / nm
AR + 0.3Cr	30	314 ± 1	228 ± 4	181 ± 32
AR + 0.8Si + 0.1V	130	336 ± 3	223 ± 3	203 ± 32
HT + 0.8Si + 0.1V	170	401 ± 2	225 ± 2	104 ± 11
HT + 1.0Si + 0.1V	160	410 ± 2	207 ± 5	121 ± 11
HT	150	409 ± 2	225 ± 2	130 ± 25

regressions in the form of neural networks. In order to do so, five different experimental ultra-high carbon rail steels have been tested under twin disc rolling contact fatigue and characterised using hardness, microscopy, and high energy synchrotron X-ray diffraction, which allows the study of solid solution strengthening as a function of the ferrite lattice parameter [14] and precipitation strengthening as a function of the phase volume fractions for increasing depths from the contact surface.

2. Experimental methods

2.1. Material, heat treatment, and sample preparation

The chemical composition of the different experimental ultra-high carbon rail steel grades used in this study are listed in Table 1. These alloys were hot rolled into 30 mm thick plates at *TATA Steel UK* and experienced a similar cooling rate to that of rail heads on cooling beds after rolling [9]. The plates were either slow cooled in still air (as-rolled, AR) or fast cooled using compressed air (heat-treated, HT) to form pearlite. Rail disc specimens, 56 mm in diameter with a contact thickness of 7 mm, were then cut out ensuring their rotational axes were perpendicular to the length of the plate to pursue constant microstructural properties such as grain size and inclusion content. The

specimens were then machined to achieve a surface roughness, R_a, at the contact surface of 0.4 μm. The same process was followed for the wheel disc specimens, but using one single pearlitic grade with composition described in Table 1, a diameter of 112 mm, contact thickness of 7 mm, and surface roughness of 0.4 μm, according to the British standard BS 970: Part 1:1983 [15].

2.2. Twin-disc RCF testing and microstructural characterisation

One sample of each grade was tested at room temperature in a twin-disc testing rig using a load of 900 MPa, a nominal slip of 5%, and water as lubricant to ensure RCF crack generation but minimal wear. Identification of crack initiation is performed by stopping each run every 10,000 cycles, removing the disc from the testing apparatus, and inspecting visually using an optical microscope. Any clear RCF crack, irrespective of size, is considered a failure so the run is terminated and the cycles recorded. In case of ambiguity, the feature in question is marked and the sample is tested for another 10,000 cycles. If the feature developed into a distinct crack, then failure by crack initiation is recorded as the previous cycle count.

After testing, radial cross sections were cut from the rail discs, mounted in bakelite, ground, polished to 0.25 μm, etched in 5% nital, and metallographically characterised using a *FEI Nova NanoSEM* (scanning electron microscope). Images of the surface were acquired for wear and rolling contact fatigue assessment, as well as from the subsurface at high magnifications for interlamellar spacing determination [16,17]. Further analysis was performed using transmission electron microscopy (TEM) with similar preparation as in [18] by first cutting 1 mm thick samples, grinding them down to ∼ 80 μm using silicon carbide paper, punching discs 3 mm in diameter, and electropolishing them using a *Struers TenuPol 5* twin jet polishing machine and a solution of 80% ethanol, 15% glycerol, and 5% perchloric acid at 19.5 V and 7 − 10 °C. TEM samples were observed in a *JEOL 200CX* microscope using a *Gatan Orius* camera and an accelerating voltage of 200 kV. The chemical composition of precipitates in the matrix of the samples was studied using energy dispersive X-ray spectroscopy (EDS) in a *FEI Tecnai Osiris* in scanning electron transmission microscopy (STEM) mode using
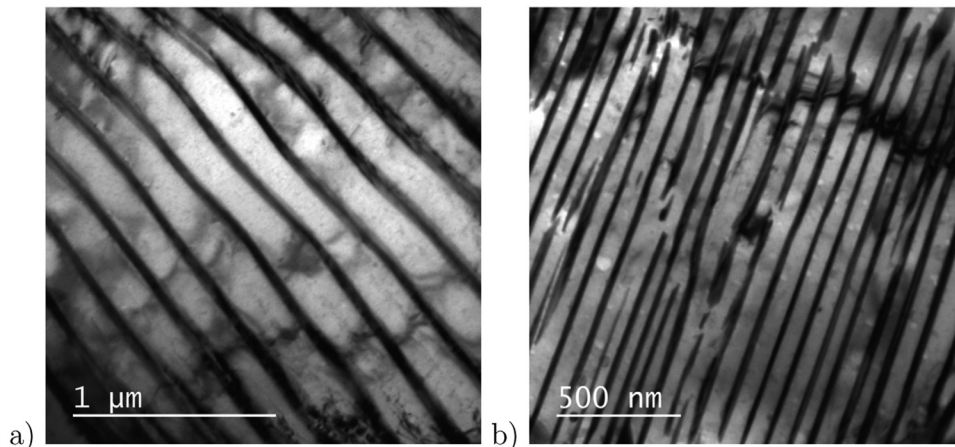

Fig. 1. TEM images of samples: (a) AR + 0.8Si + 0.1V (as-rolled, slow cooled) and (b) HT + 1.0Si + 0.1V (heat-treated, fast cooled).
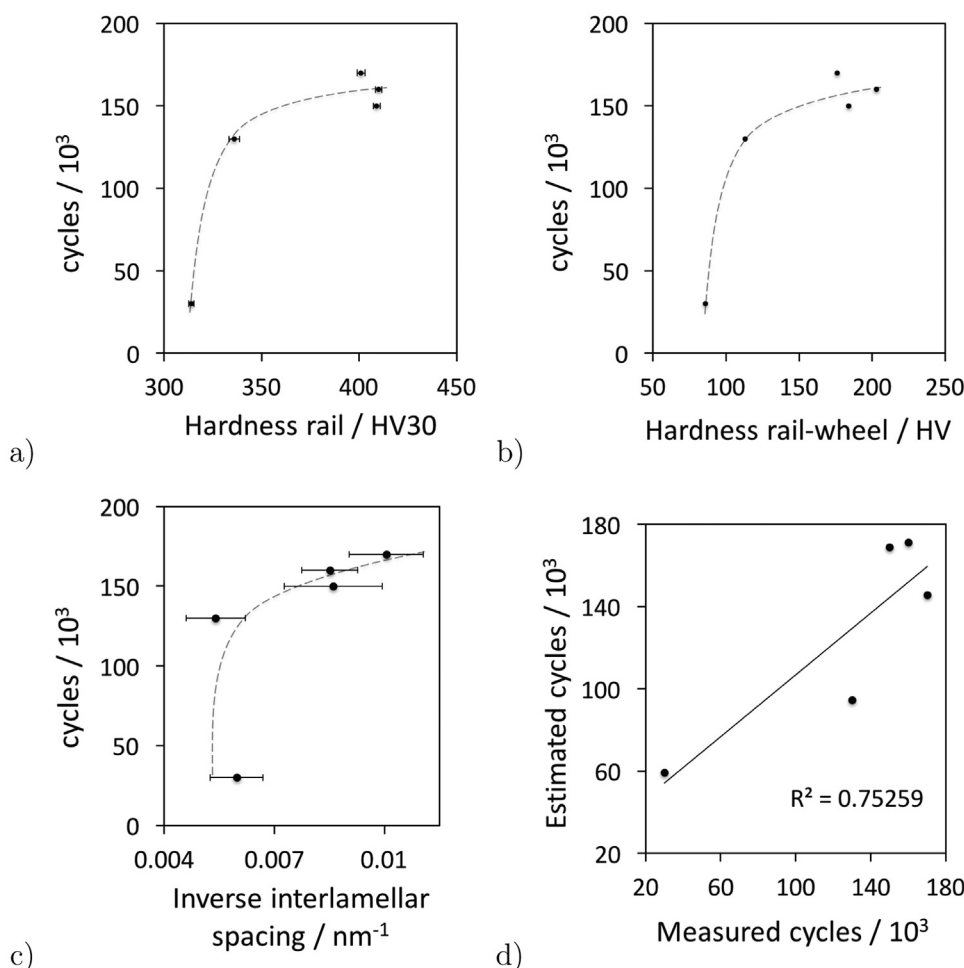
Fig. 2. Plots of (a) rail hardness, (b) rail minus wheel hardness, and (c) inverse interlamellar spacing against cycles to crack initiation, as well as (d) measured cycles against estimated values drawn from a multiple regression analysis using the rail hardness values. The curves in plots (a) to (c) are indicative of the trends in the data (not regressions).

a high-angle annular dark field (HAADF) detector and *FEI Super-X* system employing 4 *Bruker* silicon drift EDS detectors at 200 kV of accelerating voltage.

The macrohardness of the rail samples, and their corresponding wheel discs, was measured using a *Qness Q30 A +* machine by indenting the bulk of the samples ten times with a dwell time of 10 s and a load of 30 kg and 20 kg respectively.

2.3. Synchrotron measurements

High energy X-ray diffraction was performed at the *PETRA III* beamline of the Deutsches Elektronen-Synchrotron (DESY) in Hamburg, Germany. Matchstick shaped samples, 3×3 mm in cross section and 12 mm long, were cut radially from the central topmost surface of each rail disc after twin-disc testing. Each of the sides of the matchstick samples was ground with a 4000 SiC sandpaper except for the disc surface side which was just cleaned and slightly polished with 1 μm diamond paste to remove oxide debris. The length of the samples was probed in transmission using a *Perkin-Elmer XRD 1621* detector every 50 μm from the end corresponding to the disc surface down to a radial depth of 1350 μm using a monochromatic X-ray beam with dimensions 50×500 μm and a wavelength of 0.124 Å. In order to ensure adequate intensity from the cementite lamellae in the diffraction patterns collected, 25 images, each of 0.5 s exposure were summed at each position. Snapshots of a LaB_6 standard were also acquired for calibrating the measurements.

The 2-D diffraction patterns obtained were converted into 1-D intensity vs 2θ plots via azimuthal integration using *DAWN* [19]. Volume

fractions and lattice parameters of ferrite and cementite for each pattern were obtained using manually guided fitting of the Rietveld refinement [20] in *HighScore Plus* [21]. In order to study the fragmentation and eventual dissolution of cementite at the surface, which supposedly enriches the ferrite in carbon, the Rietveld refinement was performed using both cubic and body centred tetragonal ferrite as test lattices. The accumulation of strain as a function of depth, heat treatment, and composition, was investigated through polar transform plots obtained with the 'cake' function of azimuthal integration in *FIT2D* [22,23].

2.4. Neural networks

Once all the data were gathered, further analysis was performed using Bayesian neural networks [24,25]. In this framework, the neural network is used as a general form of regression where the relationship between the variables does not need to be specified but rather, is discovered. The method incorporates many techniques to automatically infer the relevance of the inputs whilst avoiding 'over–fitting'. These methods have been successfully applied to many complex relationships in materials science, including those with limited data points as is the case in the current study [26–31]. If the data are found by the method to be insufficient then the Bayesian framework indicates large uncertainties. For model training, all the data available for each parameter were compiled, not just the average values, in order to infer the correct noise level in the input data. For each set of inputs reported (hardness of rail, hardness of wheel, interlamellar spacing of rail, chemical composition of rail, volume fraction of cementite, and lattice parameter
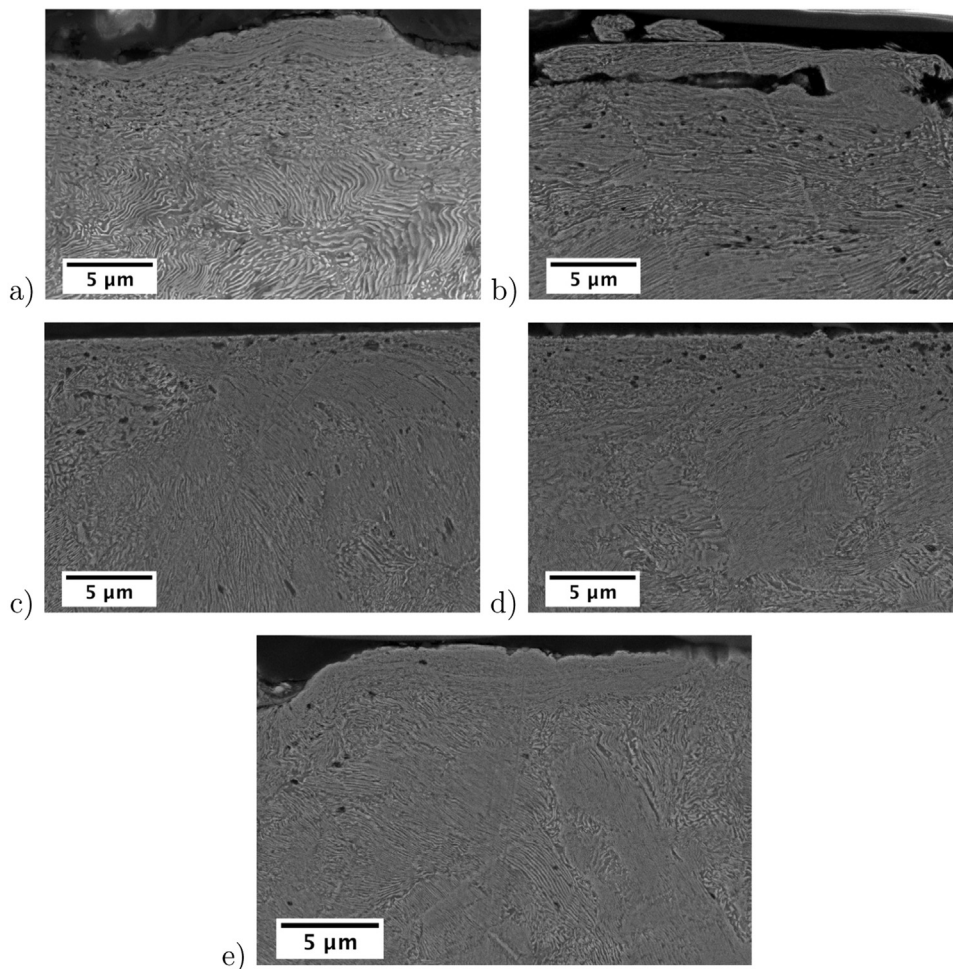
of the ferrite[1]) 180 sub-models were trained allowing a complexity of up to 20 hidden units. Nine different random seeds were used to generate the initial weights. Twenty percent of the data, corresponding to one alloy, was reserved to allow ranking and selection of the sub-models by the 'log predictive error' for subsequent incorporation into a committee model selected to produce the lowest combined uncertainty in predictions.

3. Results and discussion

3.1. Microstructural characterisation

The results from twin-disc testing and microstructural characterisation are presented in Table 2. TEM images depicting the difference in interlamellar spacing between the heat treatments using samples AR + 0.8Si + 0.1V and HT + 1.0Si + 0.1V as an example are shown in Fig. 1.

A preliminary analysis from the values obtained in Table 2 suggests that the cooling rate is the variable that mainly controls the rail hardness and interlamellar spacing. In order to then quantitatively assess which of these two properties has a greater influence on the number of cycles to crack initiation (Fig. 2), a multiple linear regression was conducted using standardised values to allow a valid comparison between variables of different units. The regression coefficient for the standardised rail hardness was 1.11 as opposed to −0.28 for the standardised inverse interlamellar spacing denoting a contribution almost four times larger of the rail hardness on the cycles to initiation than that of the inverse interlamellar spacing. Using these coefficients, estimated values of the cycles to crack initiation were obtained and plotted against measured values (Fig. 2c) to provide an approximation of the possible error associated with the values of cycles obtained, knowing that in this study each sample was only tested under RCF once due to time limitations. This is particularly relevant for AR + 0.3Cr, which seems to be a result of anomalous test conditions due to its particularly low cycles to initiation.

In an attempt to understand in more detail the variation of cycles to crack initiation, qualitative estimation of the damage mechanisms was investigated through SEM. The micrographs from the surface regions of each radial cross sectional sample are shown in Fig. 3. As seen in Fig. 3a, AR + 0.3Cr displays a considerable amount of plastic flow at the surface in conjunction with a subsurface layer of severely fragmented/possibly dissolved cementite lamellae ∼ 5 µm deep followed by ∼ 10 µm of mild cementite fragmentation.[2] These observations are consistent with the low hardness and large interlamellar spacing of this alloy. Despite a comparable interlamellar spacing and hardness (same cooling rate) as AR + 0.3Cr, sample AR + 0.8Si + 0.1V registered many more cycles than the chromium-bearing alloy. Although this is

---

[1] Interlamellar spacing, volume fraction of cementite, and lattice parameter of the ferrite were all measured 200 µm from the surface since this depth corresponds to the maximum subsurface orthogonal shear stress in twin disc line contact [32]. This should allow to estimate which of these parameters is more significant for restricting RCF damage.

[2] Whilst microscopy and hardness profiles can give a reasonable approximation of the depth of microstructural deformation, minor microstructural changes, such as rotation of low and high angle boundaries, can be perceived with crystallographic techniques such as the kernel average misorientation (KAM) angle in electron backscattered diffraction (EBSD) [33].
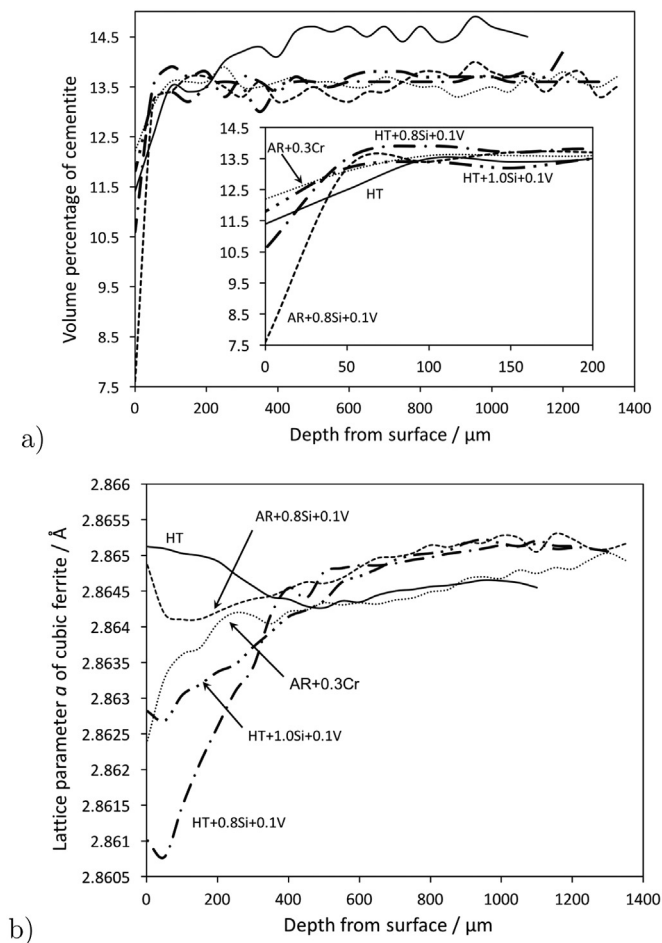
Fig. 4. Results from Rietveld refinement as a function of depth considering cubic ferrite: (a) volume percentage of cementite and (b) ferrite lattice parameter.

spacing and hardness as the other fast cooled samples. Nevertheless, these parameters did not seem to be enough to restrict plastic flow at the surface, nor severe cementite fragmentation/possible dissolution $\sim 5\,\mu m$ deep followed by another $\sim 5\,\mu m$ of mild fragmentation (Fig. 3e). Therefore, the comparison of the damage mechanisms suggests that hardness, achieved through accelerated cooling, has the largest influence on RCF resistance, but adequate alloying additions, such as Si and V, can enhance it further. By comparing AR + 0.3Cr with AR + 0.8Si + 0.1V and HT with HT + 1.0Si + 0.1V it is possible to observe that despite similar values of hardness and interlamellar spacing within each pair of samples, cycles to initiation can be altered substantially through chemical composition variations. Whereas silicon might contribute to solid solution strengthening of the ferrite that prevents cementite lamellae fragmentation by reducing strain incompatibilities and therefore, their eventual dissolution, vanadium in the form of vanadium carbides might provide precipitation hardening restricting the movement of dislocations and therefore, plastic flow. In an attempt to corroborate some of these ideas, neural network analysis of synchrotron measurements were performed to study the differences in solid solution strengthening of the ferrite through the lattice parameter and precipitation hardening through phase volume fractions as a function of depth using Rietveld refinement.

3.2. Synchrotron measurements

Due to the action of near surface shear stresses induced by rolling contact sliding, the fine pearlitic structure is expected to experience a sequence of cementite necking/thinning due to tensile fibre stresses, fragmentation caused by strain incompatibilities, and dissolution once the size becomes less than that of a critical nucleus [34–36]. Although most of the carbon atoms freed during dissolution are expected to be trapped at defects, the Rietveld refinement of the converted synchrotron data was performed using cubic (Fig. 4) and tetragonal ferrite to evaluate potential carbon enrichment.

As suspected from the SEM micrographs (Fig. 3), Fig. 4a confirms the dissolution of cementite lamellae near the surface across all five samples. However, the depth of cementite dissolution appears to differ depending on the presence or not of silicon in the alloy. The depth with respect to the surface of cementite dissolution in all three silicon-containing samples (AR + 0.8Si + 0.1V, HT + 0.8Si + 0.1V, and HT + 1.0Si + 0.1V) is $\sim 50\,\mu m$ irrespective of heat treatment, but $\sim 100\,\mu m$ for both silicon-free alloys (AR + 0.3Cr and HT).[3] Therefore, there appears to be a correlation between increasing depth of cementite dissolution, increasing degree of surface plastic deformation, and decreasing cycles to crack initiation for a given cooling rate (hardness). One important thing to note is that irrespective of Si content, most samples have a bulk cementite volume percentage of approximately 13.6%, except for HT which has 14.3% maybe due to its slightly higher C content, but this does not seem to affect the hardness, interlamellar spacing, or number of cycles for RCF cracks to form.

Another Si dependent behaviour is observed for the lattice parameter of cubic ferrite shown in Fig. 4b where the silicon-containing samples have a slightly larger bulk ferrite lattice parameter than the silicon-free ones. The fact that these values are lower than the lattice parameter of pure iron (2.8664 Å) despite the fact that silicon is responsible for a minor contraction of the ferrite lattice parameter [37], is most likely caused by a superimposed compressive elastic stress. The value of such stress was calculated to be ~ 200 MPa at the surface using the difference in cubic lattice parameters measured and the average

most likely caused by abnormal testing of AR + 0.3Cr, Fig. 3b depicts a distinct wear mode characterised by shallow cracking parallel to the running surface that ultimately detaches the heavily worn regions continually renewing the surface, which could explain the significant longer life of sample AR + 0.8Si + 0.1V. Such a difference in wear mechanism cannot be attributed to hardness or interlamellar spacing due to the constant cooling rate, but instead, it could be speculated to be related to a change in fracture toughness and fragmentation behaviour of the cementite lamellae or work hardening capacity of the microstructure caused by the silicon and vanadium additions. One important aspect to consider is that these damage mechanisms might not represent those of ultra-high carbon pearlitic steels in service since the slip of 5% used in this study is much higher than that experienced in normal wheel/rail contact ($\sim 1\%$). Also, these tests do not replicate the cyclic bending stresses at the surface and subsurface layers that actual rail experiences. However, it is important to emphasise that twin disc tests are comparator tests for many steel grades and that such comparator tests cannot be undertaken in commercial track.

A simple increase in cooling rate with a constant chemical composition in HT + 0.8Si + 0.1V compared to AR + 0.8Si + 0.1V, led not only to a halving of the interlamellar spacing and 20% hardness increase, but also negligible plastic deformation at the surface and minimal cementite fragmentation (Fig. 3c). Despite a slight increase in the silicon content, sample HT + 1.0Si + 0.1V (Fig. 3d) portrays a very similar behaviour as sample HT + 0.8Si + 0.1V (Fig. 3c) with the slightly reduced number of cycles to failure being most likely within experimental error. Accelerated cooling without the addition of elements such as silicon or vanadium in the HT sample led to comparable values of interlamellar

---

[3] It is important to bear in mind that the resolution associated to the determination of this depth is limited by the dimensions of the synchrotron beam which is 50 μm in the relevant direction. Furthermore, due to the experimental setup, the depth of the first measurement in each sample might vary slightly with respect to others, since the beam started scanning 50 − 100 μm above the sample. Therefore, the first measurement of each sample, corresponding to the surface, was decided upon the counts in the X-ray spectrum.
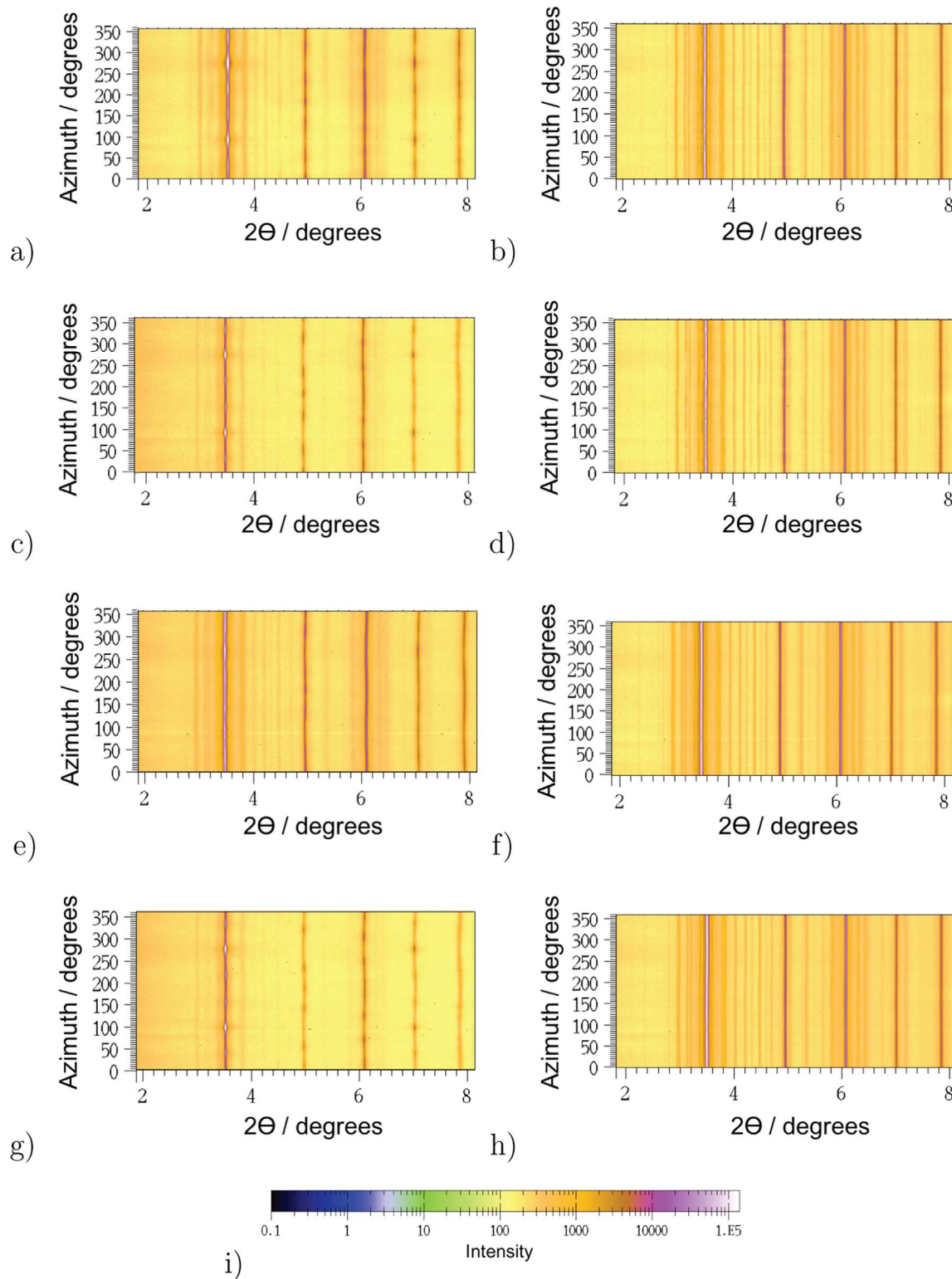
Fig. 5. Azimuthal plots of Debye-Scherrer rings obtained from: (a) AR + 0.3Cr surface, (b) AR + 0.3Cr bulk, (c) AR + 0.8Si + 0.1V surface, (d) AR + 0.8Si + 0.1V bulk, (e) HT surface, (f) HT bulk, (g) HT + 0.8Si + 0.1V surface, (h) HT + 0.8Si + 0.1V bulk, and (i) intensity scale.

Young's modulus of steel. The values of such stress would decrease with depth, explaining why, with the exception of the HT sample, there is a continuous increase of the lattice parameter for larger depths, irrespective of silicon content. It is not clear why the HT sample shows a decrease in lattice parameter up to a depth of ~ 500 µm, since the large number of cycles the sample clocked is not consistent with a tensile residual stress introduced for example through decarburisation/surface

heating due to inadequate lubrication during testing or particular conditions that would restrict the accumulation of compressive elastic stress. Just as it occurs in heavily drawn pearlitic wires, it is possible that the layers where cementite partly dissolved and ferrite was heavily deformed experienced dynamic hardening, which altered the contact conditions and wear mechanisms [38], but no experimental evidence was collected during this study to firmly resolve this aspect. At a depth

Fig. 6. STEM images and associated EDS elemental maps of the regions marked by the red squares for samples: (a) AR + 0.8Si + 0.1V and (b) HT + 1.0Si + 0.1V. (For interpretation of the references to colour in this figure legend, the reader is referred to the web version of this article.)

of 0 − 100 μm from the surface, a sudden spike in the lattice parameter occurs due to the dissolution of cementite (Fig. 4a) suggesting partial carbon enrichment of the ferrite. However, beyond that region, the trend of cementite dissolution depth with respect to silicon content using a tetragonal ferritic lattice in the Rietveld analysis was found to

be inconsistent with the microstructures observed (Fig. 3). Furthermore, the c/a ratio often resulted in values that made no physical sense because they were less than 1, which is not possible in a carbon saturated lattice. These two disparities make it clear that ferrite must be considered cubic, and not tetragonal, for this type of analysis when
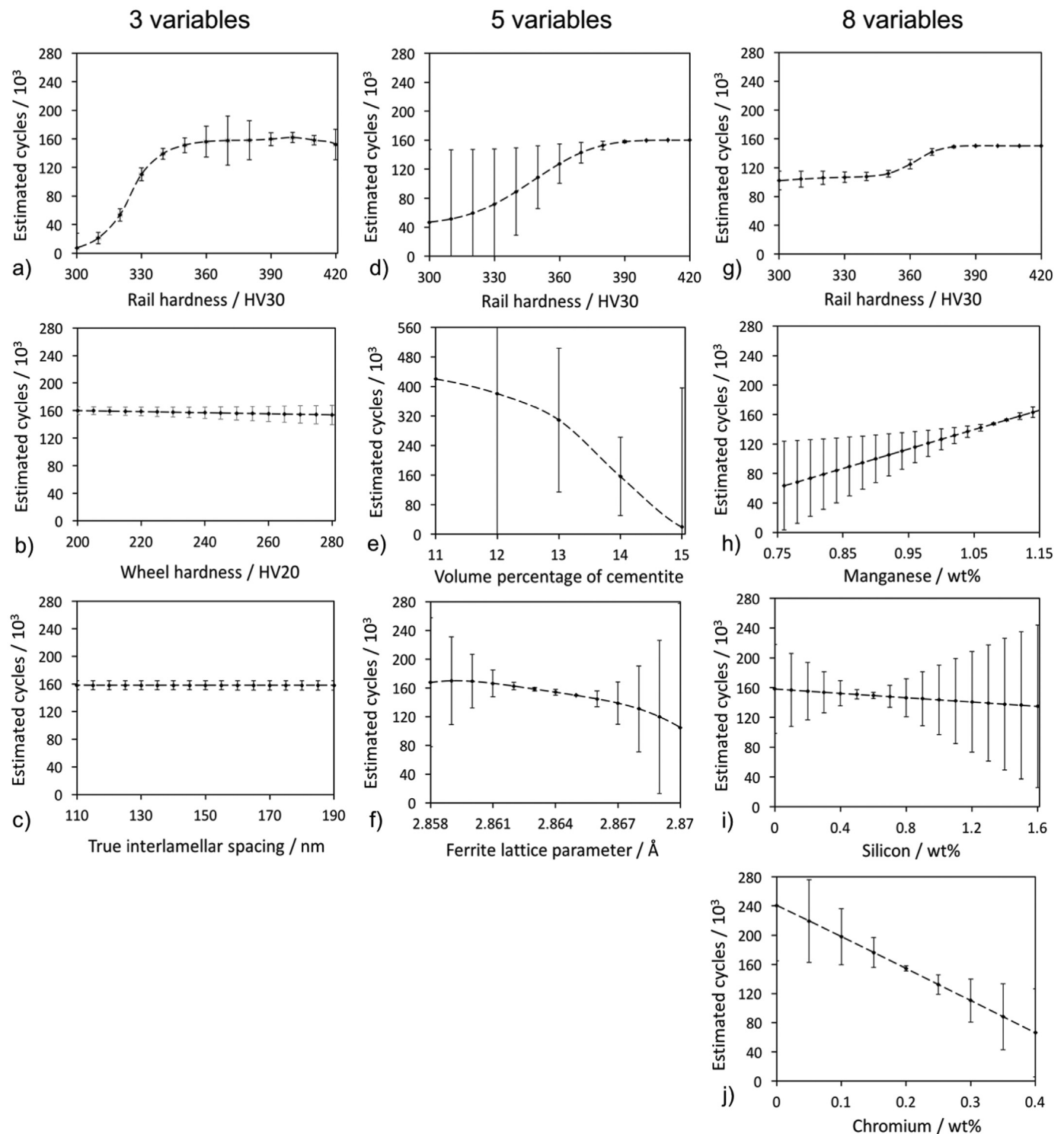
Fig. 8. Model predictions for: 3 variable model (a, b, and c), 5 variable (d, e, and f), and 8 variable (g, h, i, and j). In the 5 and 8 variable models, only the plots for the variables with trends other than constant are shown.

affects the number of cycles. Some variables, such as hardness and interlamellar spacing, are not independent, but the network indicates the separate significance of each variable. For example, interlamellar spacing, when hardness is clearly accounted for, could have a secondary influence through the thickness of the cementite layer and hence the ease with which the Fe_3C dissolves during intense elongation. Despite a substantial perceived significance of the volume fraction of cementite (Fig. 7b), the large uncertainties in the trend plot (Fig. 8e) do not allow any conclusion of a specific relationship to be made; we can only

conclude that a complex relationship exists.

With regard to chemical composition, the model suggests an increase in RCF cycles with Mn content (Fig. 8h), but a decrease in the case of Cr (Fig. 8i). Such trends refer to the effect of compositional changes independent of hardness or interlamellar spacing alterations. Due to the fact that the highest Cr-containing sample (AR + 0.3Cr) clocked very few cycles compared to the rest of the samples, most likely due to unexplained experimental abnormalities, the influence of Cr was perceived as negative by the neural network model when in practice

this element is added to increase the hardenability, even in the as-rolled condition [42]. In the case of Mn, it is included to refine the interlamellar spacing in order to increase the toughness, a property which was not quantified in this study. Furthermore, increased Mn content has not been found to lead to an improved fatigue or wear resistance in hypoeutectoid as-rolled rail steel (R260Mn) [42]. Although increasing Si (Fig. 8j) seems to decrease the RCF cycles, the large error bars above ∼0.8 wt% suggest that the model does not necessarily contradict the microscopical observations and synchrotron results, which indicated that increasing Si contents reduces the depth of cementite dissolution possibly by preventing its fragmentation in the first place due to solid solution strengthening of the ferrite and consequently, reduction of strain incompatibilities between the ferrite and the cementite. This reduction of cementite dissolution depth leads to longer RCF lives for a given heat treatment. It is emphasised that the trends deduced in the present work depend on the values of all inputs and the interpretations will therefore vary with rail type.

4. Conclusions and summary

Despite having data which only reflects a narrow window of composition and might not be extrapolated to other grades, the following conclusions can be drawn for the evidence presented:

- In twin disc lubricated tests of experimental ultra-high carbon pearlitic steels, rail hardness, attained through accelerated cooling, has a significantly larger influence on the number of cycles to crack initiation than the interlamellar spacing or wheel hardness, although adequate alloying can enhance further the rolling contact fatigue life and resistance to plastic flow. This result was corroborated by the neural network models.
- Microscopy revealed that the hard heat-treated samples displayed significantly less plastic flow at the surface and rolling contact fatigue damage than the relatively soft slow cooled ones. However, the heat treated samples which also contained Si and V displayed less plastic deformation of their surfaces and shallower depths of cementite fragmentation and dissolution in comparison with those which were only heat treated, as explained below.
- Synchrotron data confirmed the dissolution of cementite lamellae at the surface of all samples irrespective of heat treatment or chemical composition. The depth of cementite dissolution seems to be inversely related to the amount of Si in the alloy, presumably because Si strengthens the ferrite and reduces the likelihood of cementite fragmentation, and eventual dissolution, by diminishing strain incompatibilities between the two phases. Shallower depths of cementite dissolution appear to lead to longer cycles to initiation for a given cooling rate (hardness). Azimuthal plots evidenced the accumulation of anisotropic strain at the surface, and not at the depth of maximum subsurface orthogonal shear stress, most likely due to an increase in the friction coefficient caused by lubricant film degeneration due to the large number of cycles the samples clocked.
- Samples containing V displayed less plastic flow at their surfaces and longer cycles to crack initiation for a given cooling rate. The presence of vanadium precipitates was corroborated through TEM/EDS, but their size and distribution suggest that their role in rolling contact fatigue improvement could be better exploited by using for example basic oxygen steel casts in which nitrogen levels are limited to ensure adequate precipitation.
- The amount of cementite volume fraction or ferrite lattice parameter in the bulk do not appear to play a role in the number of cycles to crack initiation.

Ultra-high carbon rail steels incorporate not only accelerated cooling rates and Si contents above 0.8 wt% to prevent prior austenite grain boundary cementite, which negatively affects wear and rolling contact fatigue resistance, but also additional alloying elements such as Mn, Cr, V, and Ti, which are meant to improve performance by refinement of the interlamellar spacing, solid solution strengthening of the ferrite, and precipitation strengthening through fine carbides [1,9]. Results indicate that neither the interlamellar spacing, cementite volume fraction, or ferrite lattice parameter are the main factors behind the improved rolling contact fatigue properties. Instead, the simple increase in cooling rate and Si content, meant originally to restrict prior austenite grain cementite, were found to be the main reasons behind the improved performance of these alloys under the testing conditions of this study due to a simple increase in hardness and a decrease in the depth of cementite lamellae fragmentation and dissolution. However, other mechanisms such as V(CN) precipitation still impart incremental benefits to the wear and RCF performance of these alloys, but their effects could be maximised by limiting impurities and heat treating adequately.

References

[1] Internal report STC/PRA TRA/KR/H78991/2003/X, Tech. rep., Corus, 2003.
[2] T. Sasada, Wear research in Japan: trends and future directions, Wear 100 (1984) 561–577.
[3] D. Markov, Laboratory tests for wear of rail and wheel steels, Wear 181 (678–686).
[4] Y. Wang, T. Lei, J. Liu, Tribo-metallographic behavior of high carbon steels in dry sliding: II. Microstructure and wear, Wear 231 (1999) 12–19.
[5] R. Heyder, G. Girsch, Testing of HSH® rails in high-speed tracks to minimise rail damage, Wear 258 (2005) 1014–1021.
[6] J.H. Beynon, J.E. Garnham, K.J. Sawley, Rolling contact fatigue of three pearlitic rail steels, Wear 192 (1) (1996) 94–111.
[7] P. Pointner, High strength rail steels–the importance of material properties in contact mechanics problems, Wear 265 (2008) 1373–1379.
[8] G. Girsch, N. Frank, P. Pointner, New rail grades - a technical performance overview, in: Proceedings of the 8th International Heavy Haul Conference, Vol. Safety, Environment and Productivity, International Heavy Haul Association, Rio de Janeiro, Brazil, 2005, pp. 731–738.
[9] Internal report 136307, Tech. rep., Corus, 2008.
[10] Ordóñez-Olivares, C.I. García, A. DeArdo, S. Kalay, F.C. Robles-Hernández, Advanced metallurgical alloy design and thermomechanical processing for rails steels for north american heavy haul use, Wear 271 (2011) 365–373.
[11] Anonymous, The effect of carbide network on the life of AISI 52100 in rolling contact fatigue, Tech. Rep. May 6, Federal-Mogul Corporation, Derbyshire, U.K., 1982.
[12] P. Gembalova, J. Boruta, E. Grycz, K. M. Cmiel, Hot forming parameters research of bearing steel, Archives of Civil and Mechanical Engineering 721–28.
[13] Internal report Q2430 project 1064413, Tech. rep., TATA Steel, 2010.
[14] A. Pyzalla, L. Wang, E. Wild, T. Wroblewski, Changes in microstructure, texture and residual stresses on the surface of a rail resulting from friction and wear, Wear 251 (2001) 901–907.
[15] Anonymous, British standard specification for wrought steels for mechanical and allied engineering purposes. Part 1: General inspection and testing procedures and specific requirements for carbon, carbon manganese, alloy and stainless steels, Tech. rep., British Standards Institution, 1983.
[16] E.E. Underwood, Quantitative Stereology, Addison-Wesley Publication Company, 1970.
[17] G.F. Vander Voort, A. Roósz, Measurement of the interlamellar spacing of pearlite, Metallography 17 (1984) 1–17.
[18] W. Solano-Alvarez, H.F.G. Abreu, M.R. da Silva, M.J. Peet, Phase quantification in nanobainite via magnetic measurements and X-ray diffraction, J. Magn. Magn. Mater. 378 (2015) 200–205.

[19] M. Basham, J. Filik, M.T. Wharmby, P.C.Y. Chang, B.E. Kassaby, M. Gerring, J. Aishima, K. Levik, B.C.A. Pulford, I. Sikharulidze, Data analysis workbench (dawn), J. Synchrotron Radiat. 22 (2015) 853–858.

[20] H.M. Rietveld, A profile refinement method for nuclear and magnetic structures, J. Appl. Crystallogr. 2 (1969) 65–71.

[21] T. Degen, M. Sadki, E. Bron, U. König, G. Nénert, The highscore suite, Powder Diffr. 29 (Supplement S2) (2014) S13–S18.

[22] A. Hammersley, FIT2D: An introduction and overview, ESRF Internal Report ESRF97HA02T, ESRF, 1997.

[23] A. Hammersley, FIT2D V9.129 reference manual V3.1, ESRF Internal Report ESRF98HA01T, ESRF, 1998.

[24] D.J.C. MacKay, Bayesian methods for adaptive models, Ph.D. Thesis, California Institute of Technology, 1991.

[25] D.J.C. MacKay. Big Back, 〈http://www.inference.phy.cam.ac.uk/mackay/bigback/〉.

[26] T. Sourmail, H.K.D.H. Bhadeshia, D.J.C. MacKay, Neural network model of the creep strength of austenitic stainless steels, Mater. Sci. Technol. 18 (2002) 655–663.

[27] H.K.D.H. Bhadeshia, D.J.C. MacKay, L.-E. Svensson, The impact toughness of C-Mn steel arc-welds - a Bayesian neural network analysis, Mater. Sci. Technol. 11 (1995) 1046–1051.

[28] M.J. Peet, H.S. Hasan, H.K.D.H. Bhadeshia, Prediction of thermal conductivity of steel, Int. J. Heat Mass Transf. 54 (2011) 2602–2608.

[29] H.K.D.H. Bhadeshia, Neural networks in materials science, ISIJ Int. 39 (1999) 966–979.

[30] H.K.D.H. Bhadeshia, R.C. Dimitriu, S. Forsik, J.H. Pak, J.H. Ryu, On the performance of neural networks in materials science, Mater. Sci. Technol. 25 (2009) 504–510.

[31] H.S. Wang, J.R. Yang, H.K.D.H. Bhadeshia, Characterisation of severely deformed austenitic stainless steel wire, Materials Science and Technology 21, 2005. pp.

1323–1328. Software: 〈http://www.msm.cam.ac.uk/phase-trans/2005/thread.html〉.

[32] D.I. Fletcher, The influence of lubrication on the fatigue of pearlitic rail steel, Ph.D. Thesis, Department of Mechanical Engineering. University of Sheffield, 1999.

[33] G. Roberts, R.M. Ward, M. Strangwood, C.L. Davis, Use of misorientation values to further understand deformation in rail steels, Ironmak. Steelmak. 40 (2) (2013) 92–97.

[34] X. Sauvage, J. Copreaux, F. Danoix, D. Blavette, Atomic-scale observation and modelling of cementite dissolution in heavily deformed pearlitic steels, Philos. Mag. A 80 (2000) 781–796.

[35] D. Porter, K. Easterling, G. Smith, Dynamic studies of the tensile deformation and fracture of pearlite, Acta Metall. 26 (1978) 1405–1422.

[36] J. Languillaume, G. Kapelski, B. Baudelet, Cementite dissolution in heavily cold drawn pearlitic steel wires, Acta Mater. 45 (1997) 1201–1212.

[37] H.K.D.H. Bhadeshia, S.A. David, J.M. Vitek, R.W. Reed, Stress induced transformation to bainite in a Fe-Cr-Mo-C pressure vessel steel, Mater. Sci. Technol. 7 (1991) 686–698.

[38] Y. Li, D. Raabe, M. Herbig, P.P. Choi, S. Goto, A. Kostka, H. Yarita, C. Borchers, R. Kirchheim, Segregation stabilizes nanocrystalline bulk steel with near theoretical strength, Phys. Rev. Lett. 113 (2014) 106104.

[39] Internal report 146742 project 1064407, Tech. rep., Corus, 2009.

[40] R. Carroll, H. M. Smith, S. Jaiswal, Rail steel with an excellent combination of wear properties and rolling contact fatigue resistance, U.S. Patent 8,430,976, April 2013.

[41] P. Pointner, A. Joerg, J. Jaiswal, Definitive guidelines on the use of different rail grades, Tech. Rep. TIP5-CT-2006-031415, Innotrack project, 2009.

[42] J. Jaiswal, P. Shackleton, Crossrail RCF and wear study: Literature review and data gathering, Provided as confidential but could be made available by agreement. IRR 184/14, University of Huddersfield, 2016.